

Wall losses in straight ducts with non-circular cross sections: a scaling rule of identical losses for wooden flue organ pipes

Péter Rucz^{1,*}, Elena Esteve Fontestad², Judit Angster², and András Miklós²

¹Budapest University of Technology and Economics, Faculty of Electrical Engineering and Informatics, Department of Networked Systems and Services, 3 Műgyetem rakpart, 1111 Budapest, Hungary

²Fraunhofer Institute of Building Physics, Department of Acoustics, Group of Musical and Photoacoustics, 12 Nobelstraße, 70569 Stuttgart, Germany

Received 2 October 2024, Accepted 16 November 2024

Abstract – Viscothermal effects at the walls are the dominant sources of loss in the air columns of various types of wind instruments. The classical theory of viscous and thermal boundary layers gives an analytical result that allows for computing the wall losses of acoustical wave propagation in cylindrical ducts. Based on theoretical considerations, a simple formula is derived for straight ducts that allows for taking the shape of the cross section into account in the wall loss coefficient. This unidimensional model is compared to three-dimensional finite element computations of different geometries, and an excellent agreement is found. As an application of the theory, a revised scaling method for wooden flue organ pipes with rectangular cross sections is elaborated. In organ building practice, wooden pipes are often made narrower than the reference width because of space limitations. Organ builders reported an undesired change of timbre for narrow pipes, which may be explained by the increased amount of wall losses. The proposed scaling approach enables designing narrower wooden pipes with keeping the amount of wall losses the same as of a reference pipe. Two series of experimental organ pipes designed following the traditional and new scaling rules are examined and compared by means of acoustical measurements and sound analyses, proving the practical applicability of the proposed scaling method.

Keywords: Finite elements, Flue organ pipes, Scaling method, Viscothermal effects, Wall losses

1 Introduction

The two main sources of loss of an air column enclosed in the body of a wind instrument are sound radiation and viscothermal wall losses [1]. In case of the bores of woodwind or brass instruments and organ pipes, in general, viscothermal losses are dominant for the first few longitudinal eigenmodes [2], which have the greatest impact on the pitch and timbre of the instrument. The theory of wall losses occurring during the propagation of acoustical waves along the length of the bore is generally described by boundary layer theory [1, 3]. The analytically tractable situation is restricted to straight cylindrical ducts [4], and, as discussed in several studies (see e.g., [5–8]), the rigorous extension of the theory to slowly varying cross sections, such as cones, is non-trivial. This paper proposes a simple extension of the theory to straight tubes with constant, but non-circular cross sections, exploiting that the amount of wall losses is proportional to the ratio of the circumference and cross-sectional area of the duct. The theoretical considerations are then

validated by finite element simulations of three different practically relevant scenarios. As a practical application of the theory, a revised scaling rule for wooden organ pipes with rectangular cross-sections is elaborated and the scaling approach is examined by means of experiments on two series of pipes. The next few paragraphs briefly introduce the scaling problem of wooden organ pipes and give an overview of the structure of the paper.

The geometrical dimensions of each pipe in a newly planned pipe organ are determined in a process referred to as scaling. A so-called reference scaling method is chosen first that prescribes a geometrical progression of diameters along the notes of the musical scale. One such scale often applied in practice is the Töpfer scale [9], which assigns an inner diameter of 155 mm for the 8' C (≈ 65 Hz) diapason pipe and specifies a $1 : \sqrt[4]{8}$ ($\approx 1 : 1.682$) decrease of the diameter per octave. Then, deviations from the reference are chosen for each stop, based on the desired character of sounds for the registers with taking the room acoustic properties of the church or hall into account as needed.

*Corresponding author: rucz@hit.bme.hu

For wooden flue pipes with rectangular cross sections, two traditional scaling methods exist and both take the corresponding cylindrical pipe as a reference, as shown in Figure 1. The depth D and width W of the rectangular pipe are chosen such that they either match the diameter $2R$ of the reference pipe ($W = D = 2R$, see top right in Fig. 1), or that the cross-sectional area becomes the same as that of the reference pipe ($DW = R^2\pi$, see middle right in Fig. 1). In case of the latter method, W is chosen such that it equals a given fraction of the circumference of the reference pipe. For diapason pipes, $1/4$ is a common choice [1, 10], which gives $W = 2R\pi/4$.

The structure and parts of a wooden flue organ pipe with an open end are depicted on the left of Figure 1. Through the bore, pressurized air (referred to as “wind” in organ building) enters the pipe foot, and forms a jet as it exits the foot through the thin slit called the flue. The air jet interacts with the upper lip, resulting in the aeroacoustic generation of pressure waves that travel inside the air column of the pipe body and get reflected at the open (or closed) end. A cross-stream movement of the jet is forced by the acoustical feedback of the resonator, leading to a synchronisation of the oscillations of jet and resonator in the steady state of sound production. This process is the current understanding of the sound production mechanism of recorder-like (air reed) instruments, see e.g., [2, 11–15]. The fundamental frequency of the pipe sound is determined by the shape and length of the resonator. In case of open wooden pipes, the effective (acoustical) length can be tuned by means of the tuning slot and slide, as it is also shown in Figure 1. The geometry of the mouth region has a large influence on both the flow and acoustic radiation from the pipe [16], and hence its configuration is very important in achieving the desired perceived quality of the pipe sound. For wooden pipes, the width of the mouth is equal to the inner width of the pipe, while the height of the mouth (cut-up) is adjusted during the voicing process.

It is important to emphasize the differences between the processes called “scaling”, “voicing”, and “tuning”. In organ building practice, scaling refers to deciding the geometrical parameters of the pipe in the design phase, most importantly the (effective) diameter to (effective) length ratio, and for flue pipes, also the width and height of the pipe mouth, which are generally given in proportion to the inner circumference of the pipe. Voicing (sometimes referred to as “intonation”), on the other hand, is performed on the individual pipes first in the workshop, and then after the pipe organ is installed to its final place, and while the pipes are sounding. There are various voicing adjustments which are known to affect both the steady and transient states of the pipe sound [17, 18]. Finally, tuning refers to the adjustment of the pitch, and this process is repeated from time to time in order to keep the pipes of the instrument in tune. Since proper voicing is also necessary to attain a pleasing quality of the sound, it is practically impossible to completely separate the effects of scaling and voicing on the pipe sound.

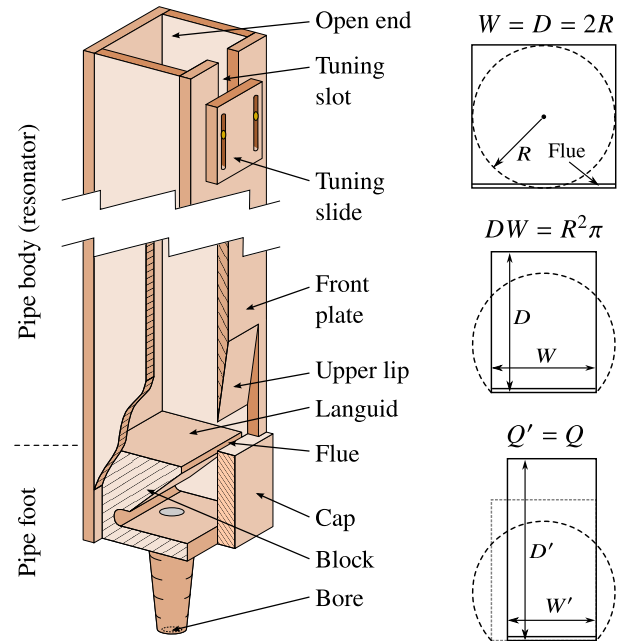


Figure 1. *Left:* parts of an open wooden flue pipe. *Right:* two traditional (*top* and *middle*) and a novel (*bottom*) scaling method.

In case of wooden pipes of the lower registers, it occurs relatively often that the pipes must be made narrower in order to fit the pipes or a whole rank of pipes into the available space. However, in practice organ builders experienced difficulties with narrow-scaled wooden flue pipes, as they reported that a narrower scaling also resulted in a noticeable and undesired change of the resulting timbre. Therefore, one of the practical problems examined in the frame of the INNOSOUND project [19] was the scaling of narrow wooden flue pipes. Instead of keeping the cross-sectional area of the pipe the same as that of the reference cylindrical pipe while decreasing its width (see the middle right sketch of Fig. 1), an alternative scaling approach was elaborated, which aims to keep the amount of wall losses and hence the quality factor Q' of the narrower pipe the same as that of the reference pipe Q (see bottom right of Fig. 1). The present paper discusses the theory of the new scaling method, and then presents experimental results of “passive” acoustic measurements and sound recordings of two series of wooden pipes, built following the traditional and the novel scaling approaches. Finite element simulations are used to supplement the theoretical analysis, as well as the acoustical modelling of complete pipes with realistic geometries¹.

The subsequent parts of this article are structured as follows. The theory of viscothermal wall losses in straight ducts with non-circular cross sections is introduced in Section 2. A finite element (FE) method that includes the effects of boundary layers as boundary conditions is

¹ It is noted that while the theoretical and experimental analysis were performed in the INNOSOUND project, advanced FE modelling was realized at a later stage.

also discussed and validated there. Three different types of cross sections are considered and the simulated wall loss coefficients are compared to the proposed theory. Section 3 introduces the experimental organ pipes made for this study. The “passive” acoustic behaviour of the pipes is examined by means of laboratory measurements and FE simulations in Section 4. The stationary and transient sound analysis of the experimental pipes are discussed in Section 5. Finally, Section 6 concludes the paper by a short summary. The subjective evaluation of the pipe sounds by two expert organ builders is also addressed briefly in Sections 5 and 6.

This article is a revised and significantly extended version of our work presented at the Forum Acusticum 2023 conference [20]. In particular, the finite element analysis of wall losses is expanded beyond rectangular ducts to triangular and elliptical cross sections. The FE modelling of complete organ pipes is extended by investigating the effect of the foot chamber in the “passive” scenario, complementing the recent studies by Tateishi et al. [21] and Ikoga et al. [22] that are based on computational fluid dynamics (CFD) simulations.

2 Methodology

2.1 Theory

Wall losses in the longitudinal propagation of acoustic waves in ducts result from friction and thermal diffusion taking place in the boundary layers developing close to the walls. In wind musical instruments, viscothermal wall losses are the consequence of the same processes [6, 8, 23]. The thickness of the viscous and thermal boundary layers are denoted by δ_v and δ_t , respectively, and are attained as:

$$\delta_v = \sqrt{\frac{2\eta}{\omega\rho_0}} \quad \delta_t = \sqrt{\frac{2\kappa}{\omega\rho_0 C_p}}, \quad (1)$$

with η , ρ_0 , κ , and C_p denoting the dynamic viscosity, equilibrium density, thermal conductivity, and the specific heat at constant pressure, respectively, and ω being the angular frequency.

The wall absorption coefficient α expresses the combined effect of the boundary layers (see e.g., [3]), and its value is found for a cylindrical duct of radius R by an asymptotic approximation [24] as

$$\alpha_o \approx \frac{1}{Rc_0} \sqrt{\frac{\eta\omega}{2\rho_0}} \left(1 + \frac{\gamma-1}{\sqrt{\text{Pr}}}\right) \approx \frac{3 \cdot 10^{-5} \sqrt{f}}{R}, \quad (2)$$

where c_0 is the speed of sound in the free field, γ is the ratio of specific heats, Pr is the Prandtl number, and f is the frequency. Hereafter the subscript \circ refers to the cylindrical geometry. The expression on the right hand side of (2) resulted from the material parameters of dry air at the ambient temperature of $T = 20^\circ\text{C}$, with expressing α_o in m^{-1} , R in m, and f in Hz units.

At low frequencies, intrinsic and radiation losses are much smaller in organ pipes than wall losses [2], thus, the

latter determine the quality factors associated with the first few longitudinal eigenmodes of the pipes. Exploiting that in practical cases $\alpha L \ll 1$ holds (with L denoting the length of the pipe), the total amount of wall losses is proportional to αL . The total amount of wall losses in a pipe is also proportional to the surface where the losses occur divided by the volume of the pipe. Hence, the damping factor ξ becomes directly proportional to the circumference C and inversely proportional to the cross-sectional area S . Similarly, the quality factor $Q = 1/(2\xi)$ is inversely proportional to C and proportional to S :

$$\alpha L \sim \xi = \frac{1}{2Q} \approx \frac{C\delta L}{SL} = \frac{C\delta}{S} \quad \text{with} \\ \delta = \frac{1}{2}\delta_v + \frac{\gamma-1}{2}\delta_t. \quad (3)$$

Therefore, the ratio of the circumferences gives the wall loss coefficient of a rectangular pipe α_o relative to that of a cylindrical pipe α_\circ as:

$$\frac{\alpha_o}{\alpha_\circ} = \frac{C_o}{C_o} = \frac{2(D+W)}{2\pi R} = \frac{1}{\sqrt{\pi}} \left(\sqrt{\varepsilon} + \frac{1}{\sqrt{\varepsilon}} \right), \quad (4)$$

where $\varepsilon = D/W$ was introduced and the effective radius $R = \sqrt{DW/\pi}$ was utilized assuming that the cross-sectional areas of the pipes are the same. From (4), it is immediately seen that $\alpha_o/\alpha_\circ > 1$ and that the minimum of this ratio is $2/\sqrt{\pi} \approx 1.128$ for $\varepsilon = 1$. By increasing ε , the ratio increases, meaning that narrowing the pipe with keeping the cross-sectional area the same increases the amount of wall losses and decreases the quality factor of the most important longitudinal modes.

It follows from (3) that in order to achieve the same quality factor, C/S must be kept constant, which allows for writing a scaling rule of equal wall losses for pipes with rectangular cross sections. Using a reference parameter $\varepsilon_0 = D_0/W_0$ that gives the depth to width ratio of a reference pipe, and a free parameter $w_n = W_n/W_0 \leq 1$ that defines a reduction of the pipe width for the new pipe, $\varepsilon_n = D_n/W_n$ is found as

$$\frac{1}{\varepsilon_n} = \frac{1 + \varepsilon_0}{\varepsilon_0} w_n - 1, \quad (5)$$

resulting in the new width $W_n = w_n W_0$ and depth $D_n = \varepsilon_n W_n$ that will give the same wall loss coefficient and quality factor as the reference pipe, i.e., $Q_n = Q_0$. In the sequel, the scaling rule (5) is applied for designing a series of pipes $n = 1, 2, \dots, 5$ with progressively decreasing w_n and W_n .

2.2 Finite element model

In this paper the FE method is applied for modelling wooden flue organ pipes with wall losses. Incorporating viscothermal wall losses into the acoustical FE technique is discussed first. The approach is validated by comparing the simulation results of straight cylindrical duct with

the classical theory. Then, three practically relevant types of cross-sections (rectangular, elliptical, triangular) are considered and the theory presented in Section 2.1 above is verified by the results of the numerical simulations. Finally, the application to real organ pipes is presented in Section 4.

An approach that enables treating the boundary layers as boundary conditions (BC) in the FE model was proposed by Berggren et al. [25]. In the simulation domain Ω , the Helmholtz equation is solved, and for the walls Γ_w the BC is written as:

$$\nabla^2 p + k_0^2 p = 0 \quad \text{in } \Omega \quad (6)$$

$$-\delta'_v \nabla_T^2 p + k_0^2 \delta'_t p + \frac{\partial p}{\partial n} = 0 \quad \text{on } \Gamma_w \quad (7)$$

where $\delta'_v = \frac{1}{2}(j-1)\delta_v$, $\delta'_t = \frac{1}{2}(j-1)(\gamma-1)\delta_t$, with j being the imaginary unit, and $k_0 = \omega/c_0$ denoting the wave number in the free field with c_0 being the speed of sound. The operator ∇_T denotes the gradient vector containing only the tangential components. To make the problem well-posed, a natural BC on the boundary of Γ_w (i.e., one or more closed curves in three-dimensional space) $\partial\Gamma_w$ is also required [25]:

$$\mathbf{n}_T \cdot \nabla_T p = 0 \quad \text{on } \partial\Gamma_w, \quad (8)$$

with \mathbf{n}_T denoting the normal vector that is aligned in the tangential direction of Γ_w .

By substituting (7) into the weak form of (6) and performing an integration by parts on Γ_w , the application of the standard Galerkin method leads to the following discretised matrix form:

$$(\mathbf{K} + \delta'_v \mathbf{K}_w) \mathbf{p} - \omega^2 (\mathbf{M} - \delta'_t \mathbf{M}_w) \mathbf{p} = -j\omega \mathbf{A} \mathbf{v}, \quad (9)$$

where \mathbf{K} and \mathbf{M} are the finite element mass and stiffness matrices, \mathbf{K}_w and \mathbf{M}_w are stiffness and mass contributions of the boundary layers on Γ_w from (7). The matrix \mathbf{A} results from a boundary term arising in the weak form of (6), while the natural BC on $\partial\Gamma_w$ (8) is transparent in the discretised form. The vectors \mathbf{p} and \mathbf{v} hold the coefficients of the pressure and normal particle velocity. In our application \mathbf{v} results from a predefined excitation and (9) is solved for \mathbf{p} in all cases discussed in the sequel.

The method discussed above was implemented in an in-house FE software package that supports both 2D axisymmetric and full 3D arrangements as well, with meshes consisting of linear isoparametric elements. In order to validate the implementation, the input impedance $Z_{in} = p_{in}/v_{in}$ of a cylindrical tube with radius $R = 10$ mm and length $L = 500$ mm was simulated first. The duct is filled by air at room temperature, and is driven by a rigid piston at the input end, and closed by a perfectly rigid termination on the other end. The input impedance was also computed by means of the transfer matrix method with applying the theory of Zwicker & Kosten [4] for the evaluation of the wall losses, referred to as the analytical solution here.

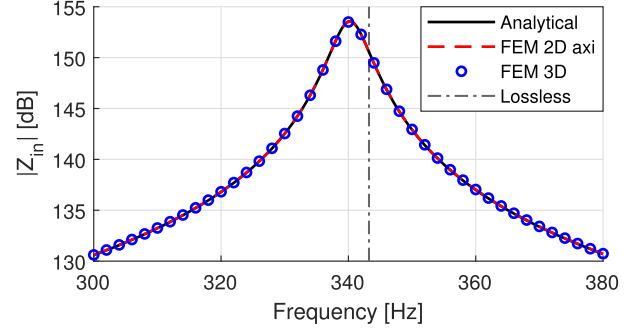


Figure 2. Input impedance of a cylindrical tube ($R = 10$ mm, $L = 500$ mm) with wall losses computed by different models.

Figure 2 compares the magnitude of the input impedance of the cylindrical tube near the first longitudinal resonance resulting from the analytical and two FE solutions. All approaches give very similar results, and as it can be expected, the frequency of the resonance peak becomes lower compared to the lossless case. The L_2 relative errors compared to the analytical solution of Z_{in} for the frequency range shown in Figure 2 is 0.41% and 0.54% for the axisymmetric and full 3D arrangements, respectively.

To compare the wall loss coefficients resulting from the FE model with the theory, a closed cylindrical duct with a radius of $R = 20$ mm was simulated first. Similar to the validation case, the duct is driven by a rigid piston at the input end and has a perfectly rigid termination at the other end. At each testing frequency, the length of the duct was taken as $L = 1.05\lambda$, with $\lambda = c_0/f$ being the wavelength in the free field. To minimize the effect of numerical dispersion, the axisymmetric model was discretised by 1000 elements along L and 20 elements along R .

The effect of the wall losses on the resulting wave number $k(\omega)$ is written as:

$$k(\omega) = k_0 + \Delta k(\omega) = k'(\omega) - j\alpha(\omega), \quad (10)$$

and hence the one-dimensional pressure field in the duct is attained as the superposition of two plane waves as

$$p(x) = p^+ e^{-jk_0 x} e^{-j\Delta k x} + p^- e^{+jk_0 x} e^{+j\Delta k x}, \quad (11)$$

where p^+ and p^- are the complex magnitudes of the forward and backward propagating waves, respectively.

In order to attain Δk from the FE results, the following procedure was utilized. Taking the pressure degrees of freedom corresponding to the nodes of the FE mesh in the axis of the duct, samples of p are found at discrete positions x_i ($0 \leq x_i \leq L$, $i = 1, 2, \dots, N$). Exploiting that $|\Delta k L \ll 1|$, the first order Taylor approximations

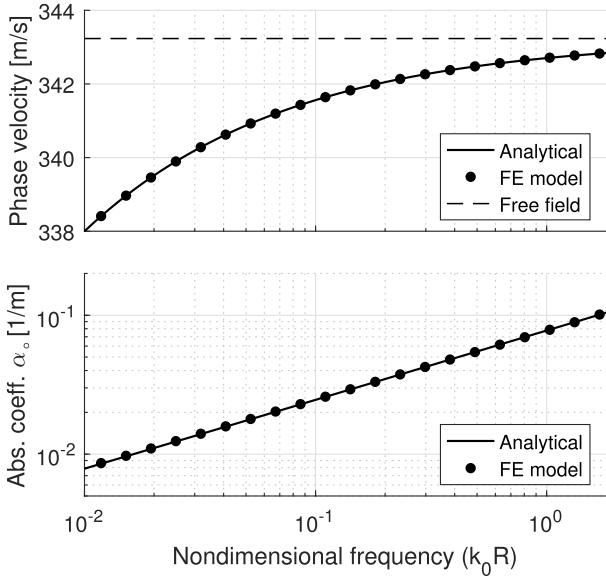


Figure 3. Frequency dependent effects of wall losses on the phase velocity $c = \omega/\text{Re}(k)$ and absorption coefficient α_o in a cylindrical tube with $R = 20$ mm.

$e^{\pm j\Delta k x_i} \approx 1 \pm j\Delta k x_i$ can be used in (11) to arrive at:

$$\begin{bmatrix} p(x_1) \\ p(x_2) \\ \vdots \\ p(x_N) \end{bmatrix} \approx \begin{bmatrix} e^{-jk_0 x_1} & e^{jk_0 x_1} & -jx_1 e^{-jk_0 x_1} & jx_1 e^{jk_0 x_1} \\ e^{-jk_0 x_2} & e^{jk_0 x_2} & -jx_2 e^{-jk_0 x_2} & jx_2 e^{jk_0 x_2} \\ \vdots & \vdots & \vdots & \vdots \\ e^{-jk_0 x_N} & e^{jk_0 x_N} & -jx_N e^{-jk_0 x_N} & jx_N e^{jk_0 x_N} \end{bmatrix} \times \begin{bmatrix} p^+ \\ p^- \\ p^+ \Delta k \\ p^- \Delta k \end{bmatrix}. \quad (12)$$

The set of equations (12) is strongly over-determined, and is solved by the least squares method, which gives an initial guess on the three variables p^+ , p^- , and Δk . Finally, this guess is refined by a non-linear least squares fit [26] with substituting x_i ($i = 1, 2, \dots, N$) into (11) and evaluating the residual (i.e., the difference of the pressure samples $p(x_i)$ and the plane wave model (11) at the positions x_i) in each iteration, starting from the initial guess.

Figure 3 depicts the comparison of the FE results and the analytical formula of Zwikker & Kosten [4] for the cylindrical pipe, showing an excellent agreement of the models regarding both the phase velocity $c = \omega/\text{Re}(k)$ and the absorption coefficient α_o . The relative difference between the analytical formula and the FE simulation is $<0.3\%$ in the frequency range of interest $0.01 \leq k_0 R \leq 1.84$. As in the finite element model the deviation of the actual wave number k from the free-field one k_0 contains both the effect of wall losses Δk and the effect of numerical dispersion (see e.g., [27]), the very good agreement with the analytical result proves that the dispersion effect is very low in the proposed approach.

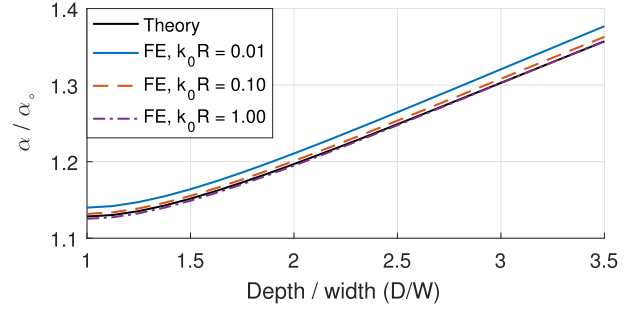


Figure 4. Wall losses of rectangular ducts as a function of $\varepsilon = D/W$. Theory (4) compared to FE.

Simulations using 3D FE models were also performed on ducts having rectangular, elliptical, and triangular cross sections and different circumference to cross-sectional area ratios. Figure 4 displays the resulting wall loss coefficients of a rectangular duct normalized by those of a cylindrical duct having the same cross-sectional area. The depth to width ratio, $\varepsilon = D/W$ was varied in the range $1 \leq \varepsilon \leq 3.5$ in 25 equal steps. At very low frequencies ($k_0 R \approx 0.01$) the FE simulation predicts slightly greater wall losses than the theory (4), with the relative difference being $\approx 1.5\%$. It is noted that these frequencies are much lower than the fundamental frequencies of the experimental pipes introduced in the next section (and that of flue organ pipes, in general), which correspond to $k_0 R \approx 0.1$. At higher frequencies $k_0 R \geq 0.1$ a very good match of theory and FE results is found with relative differences of 0.2–0.3%.

For elliptical cross sections, the ratio of the length of the major (a) and minor (b) axis was varied in the range of $1 \leq a/b \leq 5$. In case of the isosceles triangular shape, the ratio of the length of the base side (s) and the height (h) was stepped in the $2/\sqrt{3} \leq s/h \leq 10/\sqrt{3}$. Similar to the rectangular setup, 25 steps were taken in both cases. The frequency dependent results are similar to those of the rectangular geometry: at very low frequencies, the wall losses are higher in the FE simulation by 1.5 to 3.0%, and the difference diminishes to $<1\%$ in all cases near $k_0 R \approx 0.1$. Figure 5 displays the wall loss coefficients compared at the frequency $k_0 R = 0.25$ for all three geometries. Naturally, the three shapes span different ranges in C/C_o . An excellent fit of theory and FE simulations is observed with the highest discrepancy of 0.9% observed in case of the triangular geometry with high C/C_o values.

Thus, the finite element simulations confirm that the effect of non-circular cross sections on wall losses can be taken into account in a unidimensional model by scaling the wall loss coefficient of a cylindrical pipe with the same cross-sectional area by the ratio of the actual circumference and that computed from the effective radius as

$$\alpha = \alpha_o \frac{C}{C_o} = \alpha_o \frac{C}{2\pi R_{\text{eff}}}, \quad (13)$$

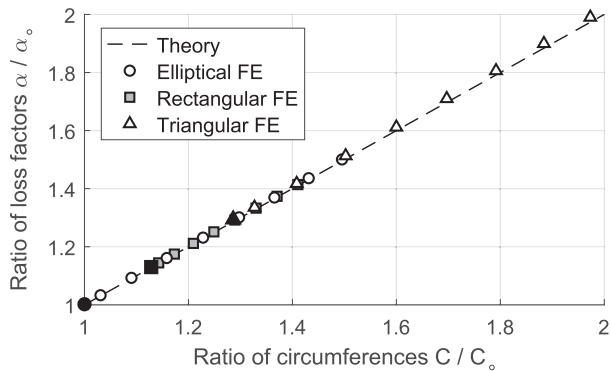


Figure 5. Comparison of theoretical and simulated wall loss coefficients α relative to the cylindrical case α_0 for different cross section shapes. Nondimensional frequency: $k_0 R = 0.25$. The highlighted black markers correspond to the circle, square, and equilateral triangle cross sections.

where the effective radius is attained from the cross-sectional area S as $R_{\text{eff}} = \sqrt{S/\pi}$. As $\alpha \sim 1/R$, scaling the loss coefficient is equivalent to using a modified radius R_{loss} for computing α making use of the theory for cylindrical ducts:

$$R_{\text{loss}} = \frac{R_{\text{eff}} C_0}{C} = \frac{2\pi R_{\text{eff}}^2}{C}. \quad (14)$$

Formulas (13) or (14) can straightforwardly be incorporated into a one-dimensional modelling framework, such as **openwind** [28], for the treatment of non-circular cross sections. Similar to the case of cones [6–8], the theory may be extended to slowly varying cross sections, e.g., pyramid shapes, which can be found in the resonators of some wooden reed organ pipes. The examination of this extension exceeds the scope of this paper.

3 Experimental pipes

For the experimental investigations, two series of wooden flue pipes were built by the company Famiglia Artigiana Fratelli Ruffatti, located in Padua, Italy. Both series consist of open pipes with a nominal tuning to $4' C$, i.e., $\approx 131 \text{ Hz}$. The pipes of the first series were scaled, tuned, and voiced by the renowned organ builder Francesco Ruffatti. The first pipe is scaled by taking the width of the mouth as $4/16$ of the circumference of a reference cylindrical diapason pipe, and the cut-up (height of the mouth) H_m is taken as $4/15$ of the width. Then, the width is decreased gradually in the series by taking $4/17$, $4/18$, $4/19$, and $4/20$ of the reference circumference as the width of the pipe, while the depth is increased such that the cross-sectional area remains the same. As the pipes become narrower, the height of the mouth was increased by the organ builder to keep the perceived loudness of the pipes roughly the same, which was achieved by setting the height of the mouth first such that the area of the mouth opening remains the same, and then slightly adjusting it during intonation.

Pipes of the second series were scaled using the scaling rule for equal wall losses (5). As a reference ε_0 was taken



Figure 6. Photo of the top view of the 1st (left) and 2nd (right) series of experimental pipes.

Table 1. Dimensions of the experimental pipes in mm units.

	Pipe	L	W	D	H_m	L_{tun}	W_{tun}
1st series	$4/16$	1180	69.8	86.9	18.6	91.3	28.2
	$4/17$	1180	64.6	93.1	21.7	107.2	25.8
	$4/18$	1181	61.2	98.3	20.6	130.4	27.1
	$4/19$	1180	58.1	103.1	23.4	128.5	26.9
	$4/20$	1179	55.3	108.4	25.1	136.5	24.1
2nd series	1	1183	70.1	87.1	20.0	0.0	30.0
	2	1183	64.9	96.6	20.0	50.0	25.8
	3	1184	60.9	105.9	22.0	68.0	26.2
	4	1185	57.8	117.1	23.0	110.0	26.4
	5	1184	55.8	128.8	24.0	148.0	26.4

as D/W of pipe “ $4/16$ ” of the first series, and the parameter w_n decreased gradually from $w_1 = 1.0$ to $w_5 = 0.8$ in steps of $\Delta w = -0.05$. The 2nd series of pipes was not voiced by the organ builder; however, the front side of the pipes were made detachable allowing for changing the cut-up H_m in voicing experiments. Since the front panels could be slid as a whole (see Fig. 1), when increasing H_m , small pieces of steel U-profiles could be inserted to fill the gap formed between the front plate and the cap on the foot. That is, the steel U-profiles substituted the missing segment of the pipe wall on the two sides of the pipe mouth when the cut-up was increased. Because of the removable fronts, tuning slots and slides were formed and installed on the back side for the 2nd series, while they were located on the front for the 1st series.

Figure 6 shows a photo of the two series of pipes beside each other, while Table 1 lists their dimensions after voicing and tuning. The parameters W_{tun} and L_{tun} are the width of the tuning slot and its length above the tuning slide. The wall thicknesses varied between 10 and 11 mm, the height of the foot was $\approx 72 \text{ mm}$, and the diameter of the foot hole was $\approx 22 \text{ mm}$ for all pipes.

4 Acoustical analysis

4.1 Transfer function measurements and simulations

The resonance properties of the pipes of the first series were examined by means of transfer function measurements in the arrangement depicted in Figure 7a. This setup enables a “passive” acoustical analysis of the resonator by means of using an external acoustic forcing instead of sounding the pipe by pressurized air coming

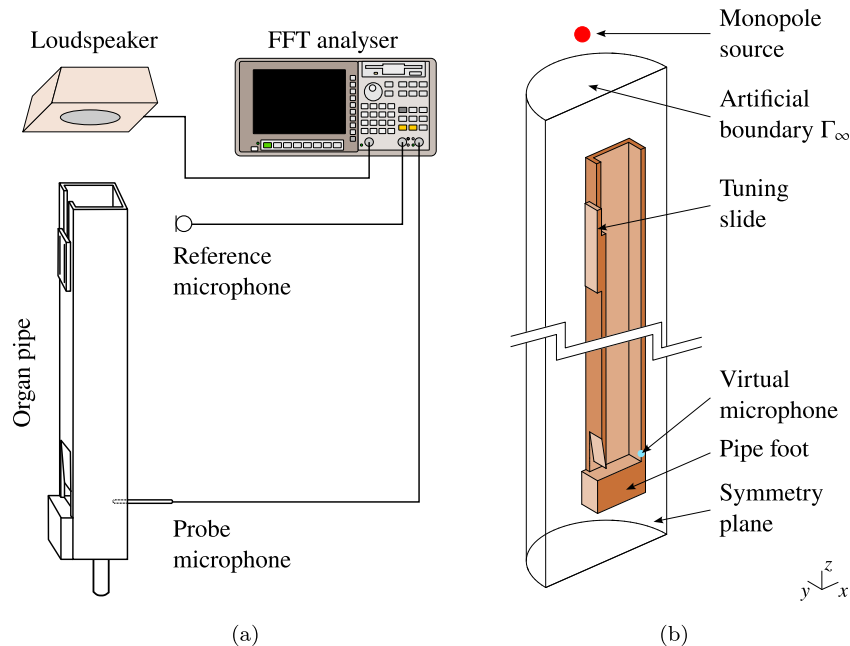


Figure 7. Transfer function measurement and simulation. (a) Measurement setup. (b) Simulation arrangement.

from the windchest. The air column inside the pipe body was excited by a loudspeaker located at a distance of ≈ 0.3 m from the open end of the pipe and driven by a logarithmic chirp signal. A B&K 4165 condenser microphone was used as a reference that recorded the excitation signal near the open end of the pipe in order to compensate for the frequency response of the loudspeaker. A small, Sennheiser KE 4-211-2 type electret probe microphone was inserted into a hole drilled into the back wall of the pipes at 10 mm distance from the languid. The excitation was provided and both microphone signals processed by a HP 35670A two-channel FFT analyser. The transfer function results from the spectrum of the probe microphone divided by that of the reference microphone.

FE simulations were also carried out, imitating the arrangement of transfer function measurements, as illustrated in Figure 7b. 3D meshes consisting of linear tetrahedron elements were created using the parametric mesh generation software *Gmsh* [29]. The typical edge length in the mesh is 10 mm inside the pipe, and it is gradually refined to 3 and 5 mm in the mouth and at the open end and tuning slot of the pipes, respectively. The acoustical simulation domain consists of the air column enclosed in the resonator as well as the surrounding free field. In the FE model, the air volume inside the pipe foot is not taken into account first, the foot of the pipe is simply cut out of the acoustical simulation domain, as if it were a solid block of wood. The effect of adding the foot chamber to the model is investigated later in Section 4.2. Free field conditions were emulated using Astley–Leis infinite elements [30], which are projected from an artificial truncation boundary Γ_∞ , i.e., the surface of a cylinder that encompasses the whole pipe and contains some of the external air. As the musically relevant range is under the

cutoff frequency of the resonator, and the first transverse mode occurs in the depth-wise direction (along the x axis in the illustration), plane symmetry along the width of the pipe ($y = 0$ plane) is exploited. The resulting FE models of the ten pipes contained ≈ 150 k elements and had ≈ 50 k degrees of freedom. The loudspeaker was modelled as a simple monopole point source, and a virtual microphone location was taken in the same position as the probe microphone inside the pipe. As the strength of the source has a unit magnitude in the model, the transfer function is attained as the frequency dependent response of the virtual microphone.

Figure 8 depicts a typical result of transfer function measurement and simulation on the example of pipe 4/18 of the first series. The series of twelve consecutive longitudinal resonance peaks is immediately identified. As it can be expected, the peaks become gradually wider and their magnitude shows a decreasing trend. Comparing the peaks to the harmonic markers (thin grey lines in the diagram), the expected stretching behaviour is observed: successive resonance peaks gradually shift toward higher frequencies from the harmonic markers. At the cutoff frequency the regular succession of the peaks breaks up due to the appearance of transversal and mixed modes. The measured and simulated transfer functions show a good agreement. In between the third and fourth longitudinal resonances, a small irregularity is observed in the measurement, which is suspected to stem from the excitation of the Helmholtz resonance mode of the air volume in the pipe foot, which was not separated from the resonator in the measurements. This speculation is investigated in more detail in Section 4.2. While the simulation predicts monotonically decreasing magnitudes of the first ten peaks (except for the first peak), the measurement

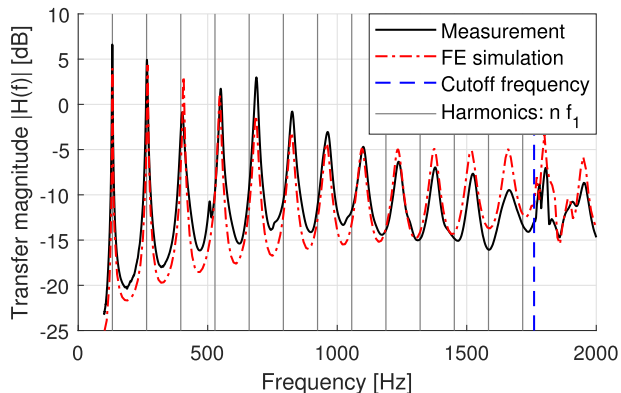


Figure 8. Comparison of measured and simulated transfer functions. (Pipe $4/18$ of the first series.)

exhibits some irregularities, e.g., the third peak has a locally minimal, while the fifth peak has a locally maximal magnitude. The average deviation between the magnitudes of the peaks in the measurement and the simulation is ≈ 1.9 dB, while the maximal difference is 4.2 dB.

The quality factors and the natural frequencies were found by fitting resonance curves onto the narrow neighbourhood of the peaks of the measured and simulated transfer functions $H(f)$:

$$|H(f)|_i \approx \left| \frac{A_i f_i^2 / Q_i}{f_i^2 + j f_i f / Q_i - f^2} \right|, \quad (15)$$

with $i = 1, 2, \dots, 10$ denoting the i th peak and A_i , Q_i , and f_i being the corresponding magnitude, quality factor, and eigenfrequency, respectively. The approximation of (15) only holds near the resonance peaks (denoted by the i subscript of $|H(f)|$), if the quality factor Q_i are sufficiently high, and the peaks are well-separated in frequency. As the average of the coefficients of determination resulting from the fits were >0.99 for all five pipes, the approximation can safely be accepted. The cutoff frequency, i.e., the frequency of the first depth-wise transverse mode, $f_{\text{cut}} \approx c_0 / (2D)$ is also found from the transfer functions, as shown in Figure 8.

Table 2 displays the measured and simulated resonance properties of the fundamental modes and cutoff of the first pipe series. While the eigenfrequencies show an excellent agreement, the FE model gives 18–29% higher Q values than the experiments. A possible explanation of this deviation is the presence of further sources of loss in the measurement, which are not accounted for in the numerical model, such as the roughness of the wall surfaces and the vibration of the walls. The approximation of (3) gives Q_1 values from 69.2 (pipe $4/16$) to 65.5 (pipe $4/20$). All three methods gave a decreasing Q_1 value as D/W increases, with the measurement showing the largest decrease in Q_1 . The resulting cutoff frequencies agree well with the theoretical values, and f_{cut} being inversely proportional to D is also observed.

The frequencies of the first 10 peaks were also compared, and an excellent agreement was found with relative

Table 2. Measured and simulated resonance properties of the first series of pipes.

Pipe	Measurement			Simulation		
	f_1 [Hz]	Q_1 –	f_{cut} [Hz]	f_1 [Hz]	Q_1 –	f_{cut} [Hz]
$4/16$	130.9	66.3	1987	130.8	78.7	1990
$4/17$	131.0	67.4	1848	132.0	78.3	1844
$4/18$	131.7	65.5	1740	132.2	76.8	1760
$4/19$	131.9	63.0	1664	132.6	76.9	1678
$4/20$	131.7	59.4	1582	132.2	76.1	1596

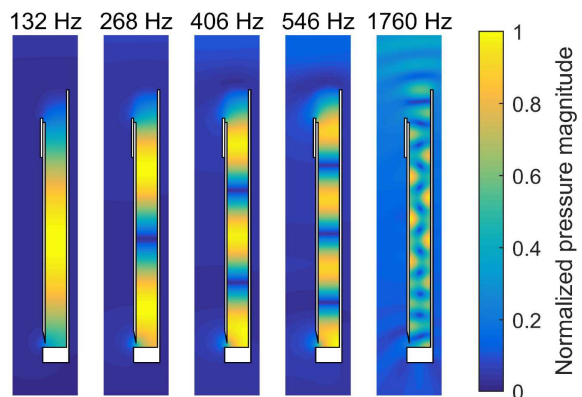


Figure 9. Simulated pressure waveforms of pipe $4/18$ at the first four resonance frequencies and at the cutoff.

differences of 1.2% maximum and $<0.5\%$ average. Thus, the FE method with wall losses and infinite elements proves to be a suitable tool for predicting the resonance properties of flue organ pipes. The FE simulation also highlights the importance of wall losses for the first few longitudinal modes of the resonator. A simulation without wall loss effects results in Q_1 values that are more than three times greater than that with wall losses. At higher frequencies, radiation losses become dominant and the discrepancy between the models with and without wall losses diminishes: above 1 kHz, the difference in Q values is only 10–12%.

Figure 9 displays the first few longitudinal standing wave shapes of pipe $4/18$ and the effect of the cutoff. As typical to organ pipes with an open end, the pressure maxima of longitudinal modes are shifted slightly towards the mouth from the center of the pipe, as a consequence of the radiation impedances being different at the two openings [31]. The asymmetric radiation pattern due to the presence of the tuning slot is also visible near the open end of the pipe.

It has to be mentioned that transfer function measurements were only carried out on the first series of pipes, partially as a consequence of the voicing procedure of the second series. As the geometries of the latter pipes were adjusted during sound recording experiments, we failed to capture their final setup in transfer measurements.

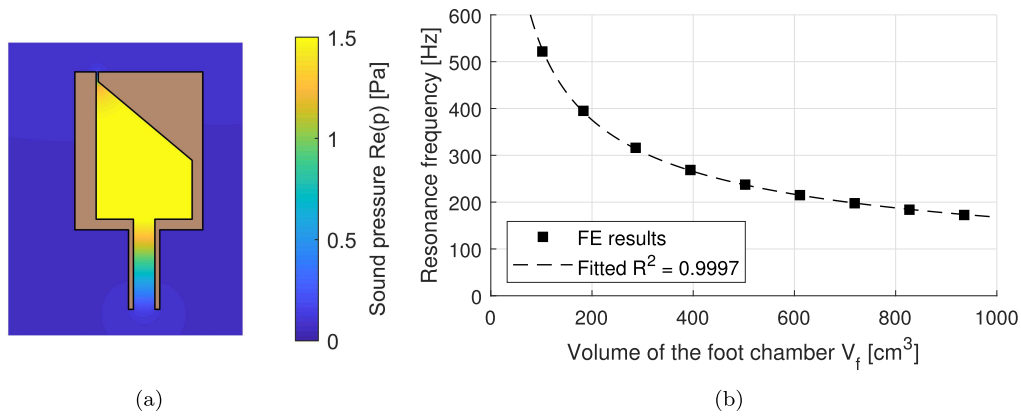


Figure 10. Helmholtz resonance in the pipe foot. (a) Sound pressure in the foot at resonance. (b) Resonance frequency as a function of the volume V_f .

4.2 The effect of the pipe foot

The effect of the foot chamber on the sound production by a closed organ pipe was studied by means of computational fluid dynamics (CFD) in recent publications [21, 22]. The latter studies showed that the resonances in the foot chamber can affect the motion of the air jet and the efficiency of the aeroacoustic excitation of the resonator by the jet. Here, the effect of the acoustical coupling between the pipe foot and the pipe body on the transfer function is examined by means of finite element simulations. First, simplified models containing only the pipe foot were created. In these models, the complete resonator is omitted and the arrangement contains the air inside the foot chamber, flue, and bore, as well as a small region of the external air to allow for the application of infinite elements.

At low frequencies, where the length, depth, and width of the foot chamber are all significantly smaller than the half of the acoustical wavelength, the pipe foot can function as a Helmholtz resonator, with the air enclosed in the foot chamber representing the volume, and the flue and bore (see Fig. 1) taking the role of two necks. The combined effect of the two necks can be described by their effective cross section S_{eff} and length L_{eff} . The latter incorporates the end corrections of both the flue and bore resulting from the radiation into the free field. Thus, the Helmholtz resonance frequency f_H depends on the effective parameters and the volume of the foot chamber V_f as

$$f_H = \frac{c_0}{2\pi} \sqrt{\frac{S_{\text{eff}}}{V_f L_{\text{eff}}}}. \quad (16)$$

Similar to the case of transfer function simulations, the foot chamber was excited by a monopole source and the response was taken in the bottom front corner of the foot chamber. The simulations were performed using nine different geometries with increasing the volume of the foot chamber V_f gradually by changing its length L_f . Hereafter, L_f denotes the inner length of the foot chamber, measured from the top exit of the flue to the top of the bottom plate of the pipe foot. The inner width and depth of the foot chamber are the same as of pipe ⁴/₁₈, i.e.,

$W = 61.2$ mm and $D = 98.3$ mm. The flue channel has a length of $L_{\text{flue}} = 10.0$ mm and its width is $d_{\text{flue}} = 2.2$ mm, while the bore has a length of $L_{\text{bore}} = 92.4$ mm and inner diameter of $d_{\text{bore}} = 22.0$ mm. The angle of the inclined plane inside the foot chamber is $\beta_f = 50^\circ$ measured from the vertical plane, see Figure 10a.

A single resonance peak was found under the cutoff frequency of the foot model in each case. Figure 10a exemplifies the pressure field in the pipe foot at the resonance frequency ($L_f = 161.8$ mm and $f_H = 215$ Hz in this case). As observed, the sound pressure has no spatial dependence inside the chamber, significant gradients are observed in the flue channel and the bore, which confirms that the foot acts as a Helmholtz resonator. As it is seen in Figure 10b, by increasing V_f , the resonance frequency f_H decreases monotonically. Furthermore, a curve inversely proportional to $\sqrt{V_f}$ gives an excellent fit to the frequencies with a coefficient of determination of $R^2 = 0.9997$, which also supports that the resonance in the foot chamber is of the Helmholtz type. At higher resonance frequencies (smaller V_f) the actual frequencies are very slightly higher than those resulting from the fit, while at smaller frequencies (greater V_f) it is the other way around. This behavior can be explained by the effective length L_{eff} of the necks being slightly smaller at higher frequencies due to the frequency dependence of the end corrections at both openings.

A complete FE model containing both the pipe body and the foot was also created in order to examine the coupling of the two parts. The model of pipe ⁴/₁₈ was extended by the foot, with $L_f = 71.9$ mm and the other dimensions being the same as given above. An alternative model with a longer foot of $L_f = 123.5$ mm was also set up. While the former model is the realistic one, the Helmholtz resonance of the foot chamber with the longer foot is expected to interact with second longitudinal mode of the air column inside the pipe body.

The results of the two models are compared with the measurements in Figure 11. With incorporating the pipe foot with the real $L_f = 71.9$ mm the small irregularity near 500 Hz appears in the simulated transfer function (red dash-dotted curve), corresponding to the Helmholtz resonance inside the foot chamber. The frequency of the

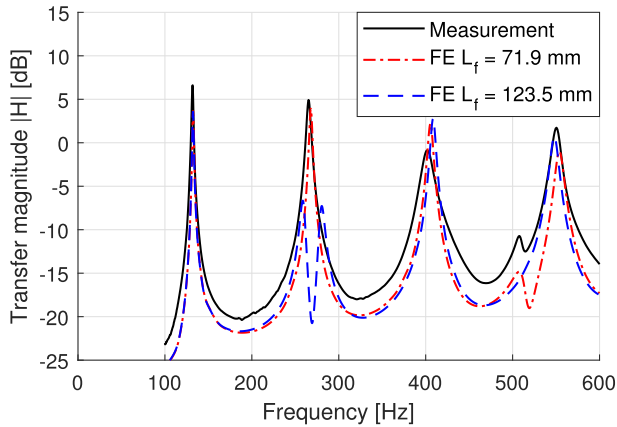


Figure 11. Comparison of transfer function measurement of pipe $4/18$ with FE models containing both resonator and pipe foot.

small peak is 508 Hz both in the measurement and the simulation. The simulation predicts a slightly sharper dip between the Helmholtz resonance in the foot and the fourth longitudinal mode of the pipe. With increasing the length of the foot to $L_f = 123.5$ mm, the volume of the pipe foot increases to ≈ 390 cm³ and the Helmholtz frequency becomes close to 265 Hz, see Figure 10. Confirming the expectations, the FE simulation (blue dashed curve in Fig. 11) shows a strong interaction of the pipe foot and the second longitudinal mode of the resonator, with the resonance peak split into two. The split of the resonance peak is explained by the avoided crossing phenomenon: when the frequencies of two modes become close, they repel each other, and the two degenerate modes split into two modes, with one having a lower and the other a higher frequency than the original mode. A good example of this phenomenon in musical acoustics was given by Adachi [32, 33] for the case of playing cross-fingered notes on the tenor recorder. In the present case, the first mode appears at 258 Hz, and the pressure oscillations in the foot chamber are in phase with those in the lower (closer to the foot) part of the resonator, while the second mode with opposite phases appears at 280 Hz. At the same time, near the frequency of the second longitudinal mode (≈ 265 Hz for $L_f = 71.9$ mm) a local minimum of the transfer function appears in this case. From a practical perspective, it seems that a strong acoustical coupling of resonances inside the foot and the pipe body is better avoided in order to prevent the splitting of the first few longitudinal modes that have an important role in forming the character of the pipe sound.

Simulations with including the pipe foot in the model agree with the results of the CFD studies [21, 22], i.e., they confirm that the foot chamber acts as a Helmholtz resonator. Transfer function simulations highlight that the coupling of foot chamber and resonator is of acoustic nature and also affects the “passive” characteristics of the pipe. The proposed FE methodology seems an efficient tool for identifying undesired strong coupling of foot and resonator in the design phase.

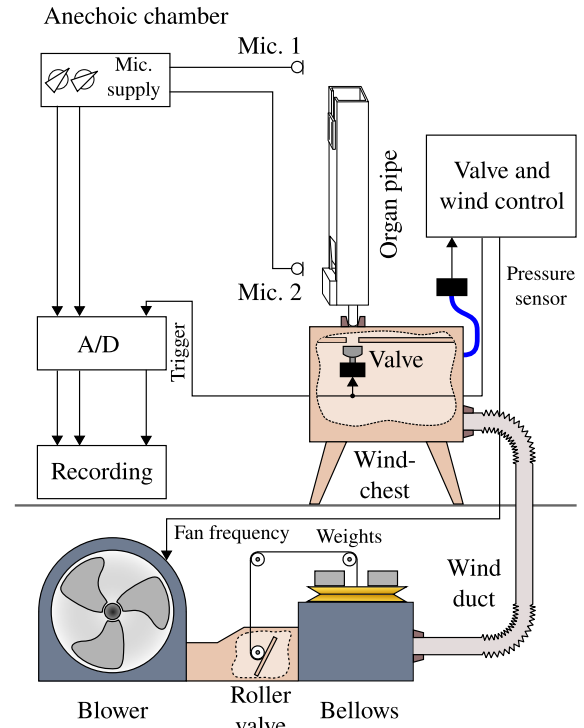


Figure 12. Measurement arrangement of sound recordings.

5 Sound analysis

The sounds of the experimental pipes were measured and recorded in the anechoic room of the Fraunhofer Institute of Building Physics, Stuttgart, Germany using the setup illustrated in Figure 12. A wind system including the blower, regulator, and wind ducts was assembled outside the anechoic room and the wind duct was lead into the measurement chamber and connected to the windchest. A windchest pressure of 700 Pa was utilized for all recordings, which corresponds to the voicing wind pressure for the 1st series of pipes. The opening of a time-controlled valve in the windchest made the pipes sound and served as the trigger signal of the measurement as well. Two calibrated $1/2''$ condenser microphones (type B&K 4165) were placed near the open end and the mouth of the pipes. After amplification, the microphone signals were sampled at $f_s = 44.1$ kHz rate by an 16-bit RME Hammerfall DSP sound card connected to a portable computer.

Three 10 s-long sounds were captured with 5 s pause between them in each case. The steady states were first analysed, and the fundamental frequencies f_1 of the pipe sounds were determined. Then, the recordings were re-sampled at a new rate of $f'_s = 64f_1$ and the steady state spectra and attack transients were evaluated. Re-sampling is beneficial for attaining a high signal-to-noise ratio and avoiding the spectral leakage and picket fence effects in the steady state sound. In the attack stage it allows for extracting the accurate magnitudes of the harmonic partials even in short time windows. In the

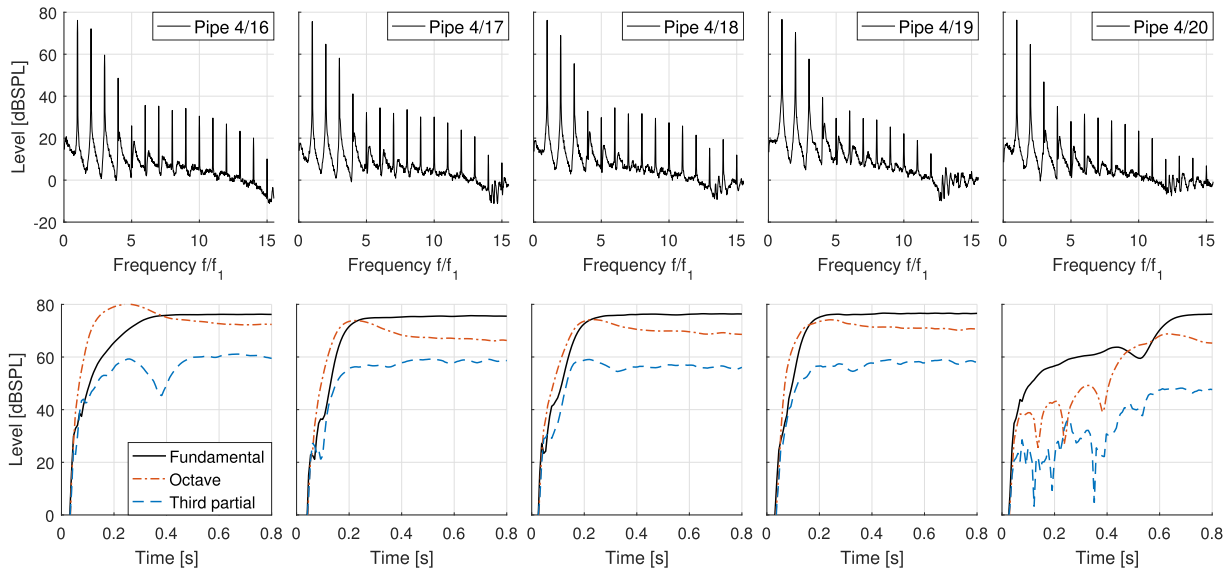


Figure 13. Stationary spectra and attack transients at the mouth for the first pipe series, $f_1 = 131$ Hz.

sound evaluations presented in the sequel, the parameters of the spectral analysis were chosen as follows. Window sizes were set to 4096 and 256 samples in the steady and attack transient stages, respectively, while a 75% overlap of successive windows was used in both types of analyses.

Figure 13 displays the steady state spectra and attack transients of the first pipe series, measured near the mouth of the pipes. A normalized frequency scale is utilized, where the fundamental frequency is $f_1 = 131$ Hz in all cases. All pipes in the first series have only a few strong partials: beside the fundamental the octave and the third partial (perfect fifth) are relatively strong, and the higher partials are significantly weaker. The attack transients of pipes 4/17, 4/18, and 4/19 are very similar to each other. In each case, the octave has a larger magnitude in the initial stage, and the steady state magnitudes of the first three partials are reached after ≈ 0.4 – 0.5 s which corresponds to 50–65 periods. For pipe 4/16, a larger overshoot of the octave is observed in the attack transient. The attack of pipe 4/20 became very slow, ≈ 0.8 s was needed to reach the steady state magnitudes. In contrast with the previous pipes, the fundamental develops first, and the magnitudes of all three strong partials fluctuate during the attack, which can be attributed to the high cut-up.

The opinion of the organ builder on the first series of pipes was that the colour of the sound gradually gets “darker” (more fundamental, less upper harmonics), which he expected due to decreasing the width and increasing the cut-up. By increasing the cut-up, the flue to upper labium distance becomes greater, and hence, the frequency of the edge tone (or mouth tone) decreases [34, 35]. The latter effect and the increased amount of wall losses both contribute to the diminishing harmonic content. The organ builder also remarked that with increasing the depth, the acoustical length of the pipe seems to

increase. Notice that the length of the tuning slit L_{tun} had to be increased gradually to compensate for the increase of the effective length and achieve the same pitch, see Table 1.

As the 2nd series of pipes was not voiced by the organ builder, we pursued the following procedure. First, the attack transients were recorded and evaluated with different heights of the mouth, exploiting the detachable front sides of the pipes. The attack transients were found to be pleasingly similar for cut-up heights of 20, 20, 22, 23, and 24 mm for the five pipes, respectively. Then, the pipes were tuned to the same fundamental frequency of 126 Hz using the tuning slides, resulting in tuning slot lengths of 0, 50, 68, 110 and 148 mm, respectively. Finally, new sound recordings were made for sound analysis.

Figure 14 depicts the resulting stationary spectra and attack transients. The close similarity of the levels of the first three partials in the steady state is immediately observed across the first four pipes. The attack transients are similar to those of the 1st series: the octave becomes the strongest partial in the initial stage. It has to be remarked that the voicing by the organ builder resulted in quicker attacks and less fluctuation of the levels of the partials.

Table 3 summarizes the levels of the first three partials in the steady state sound of each pipe. The professional voicing resulted in very similar levels of the fundamental for the first series of pipes, while in the second series the differences are somewhat higher. At the same time, the relative level of the octave exhibits larger variations in the first series. In both series, the last pipe (#5) can be considered an outlier, as the 3rd partial became remarkably weaker for these pipes. For the second series of pipes, the fundamental also became significantly weaker, and hence, the equivalent loudness of this pipe also decreased. Concerning the similarity of the first four pipes, the new scaling method can be regarded successful.

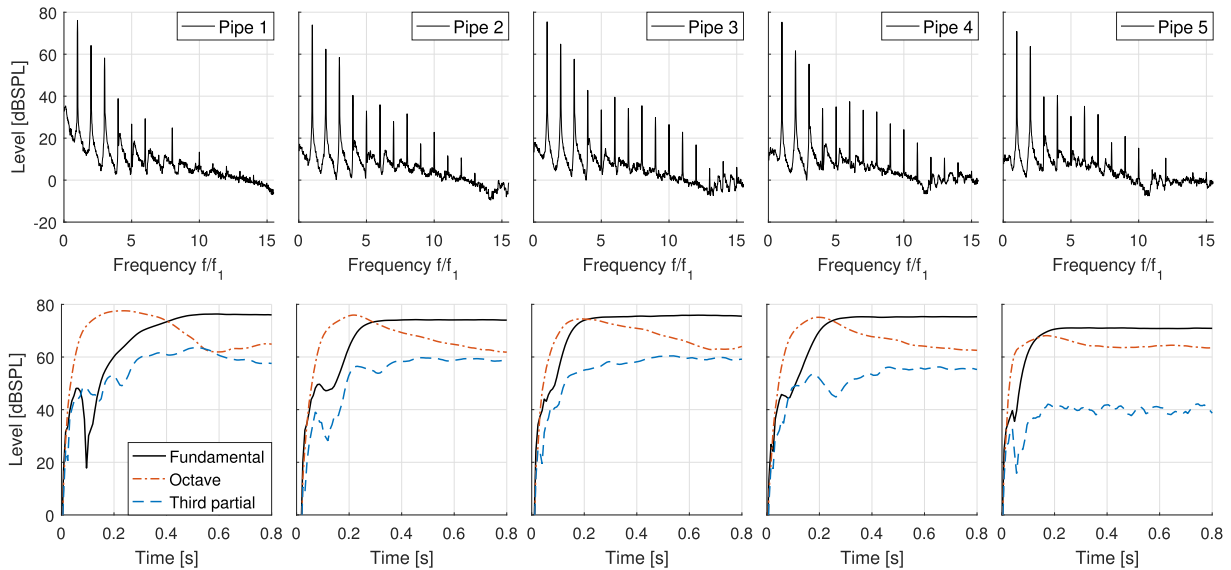


Figure 14. Stationary spectra and attack transients at the mouth for the second pipe series, $f_1 = 126$ Hz.

Table 3. Absolute level of the fundamental (L_1) and relative levels of the octave and third partials (ΔL_2 , ΔL_3) in the steady state. Values are in dB SPL.

Pipe	1st series			2nd series		
	L_1	ΔL_2	ΔL_3	L_1	ΔL_2	ΔL_3
#1	76.2	-4.0	-16.5	76.1	-12.0	-17.9
#2	75.5	-10.8	-17.4	73.9	-11.5	-15.5
#3	76.1	-7.2	-20.7	75.4	-10.6	-17.8
#4	76.6	-6.3	-18.9	75.2	-13.7	-20.0
#5	76.2	-11.6	-29.5	70.8	-7.2	-31.1

6 Discussion

This paper considered a practical extension of wall loss models of wind musical instruments that allows for taking the effect of non-circular cross sections into account. As an application of the theory, a possible improvement to the scaling of wooden flue organ pipes with rectangular cross sections was examined. The general idea of the proposed scaling method was to keep the amount of wall losses constant opposed to keeping the cross-sectional area constant when reducing the width of the pipe. The theory of wall losses in a straight duct having a rectangular cross section was reviewed and a new scaling rule (5) was established. Simulations of pipe models by means of the acoustical finite element method were also performed, relying on a recent technique for the incorporation of viscothermal wall losses. Very good agreement of the theoretical analysis and the computational model was observed, both for the cylindrical shape and three other, practically relevant cases: rectangular, elliptical, and triangular cross sections. It is straightforward to incorporate the theoretical results (13) and (14) into one-dimensional computer models of wind instruments.

Two series of experimental pipes using the traditional and new scaling methods were manufactured and analysed by means of laboratory experiments and numerical models. Comparing transfer function measurements and simulations of the first series of pipes gave a promising agreement of the resonance properties. By including the pipe foot in the computational model, minor irregularities observed in transfer function measurements could be reproduced by finite element simulations. Furthermore, in agreement with previous CFD studies [21, 22], the numerical results confirm the possibility of exciting the Helmholtz mode of the foot chamber, and also show that a strong acoustical coupling of the foot and resonator can occur. The case study also revealed that unfavourable choices of the dimensions of the foot can result in an undesirable splitting of one of the longitudinal modes of the resonator. Sound recordings were made on all experimental pipes using a realistic wind system. The steady state and transient analysis of the recordings showed that it is possible to maintain the similarity of the timbre and attack of progressively narrower pipes by applying the proposed scaling method.

The importance of the effect of voicing on the resulting pipe sound has to be emphasised here. After an experienced organ builder and voicer, Konrad Mühleisen (Werkstätte für Orgelbau Mühleisen GmbH, Leonberg, Germany) listened to the sounds of the 2nd series of pipes, he immediately objected the slowness of the attacks. He recommended various further voicing adjustments, such as attaching beards to some of the pipes. Nevertheless, he reconsidered his opinion on designing narrower wooden flue pipes with similar timbres from “impossible” to “possible”, with further modifications.

In the end, some remarks are made on the application of the proposed method. As an example, the total width of a 8' rank of diapason pipes with 3 octaves (37 pipes from 8' C₂ to 1' C₅) can be reduced from ≈ 2.95 m to ≈ 2.51 m,

with taking $w = 80\%$. The same method may be applied for designing stopped wooden flue pipe ranks.

Acknowledgments

The research was financially supported by the European Commission in the frame of the “INNOSOUND” project (Grant Agreement Ref. No. 222104). Contributions of Francesco Ruffatti (preparation of experimental pipes) and Konrad Mühleisen (participation in voicing experiments) are gratefully acknowledged. The open access publication of this work has been supported by the Hungarian National Research, Development and Innovation Office under contract No. K-143436.

Conflicts of interest

The authors declare that they have no conflicts of interest in relation to this article.

Data availability statement

The data presented in the paper are available from the corresponding author on request.

References

- N.H. Fletcher, T.D. Rossing: The physics of musical instruments, 2nd edition. Springer, New York, 1998.
- A. Miklós, J. Angster: Properties of the sound of flue organ pipes. *Acustica-Acta Acustica* 86, 4 (2000) 611–622.
- E.L Kinsler, A.R. Frey, A.B. Coppens, J.V. Sanders: Fundamentals of acoustics, 4th edition. John Wiley & Sons, Inc., 2000.
- C. Zwicker, C.W. Kosten: Sound absorbing materials. Elsevier, 1949.
- Y. Kulik: Transfer matrix of conical waveguides with any geometric parameters for increased precision in computer modeling. *Journal of the Acoustical Society of America* 122 (2007) EL179–EL184. <http://dx.doi.org/10.1121/1.2794865>.
- A. Ernoult, J. Kergomard: Transfer matrix of a truncated cone with viscothermal losses: application of the WKB method. *Acta Acustica* 4, 2 (2020) 7. <http://dx.doi.org/10.1051/aacus/2020005>.
- T. Grothe, J. Baumgart, C.J. Nederveen: A transfer matrix for the input impedance of weakly tapered, dissipative cones as of wind instruments (L). *Journal of the Acoustical Society of America* 154, 1 (2023) EL463–EL466. <http://dx.doi.org/10.1121/10.0020270>.
- A. Thibault, J. Chabassier, H. Boutin, T. Hélie: Transmission line coefficients for viscothermal acoustics in conical tubes. *Journal of Sound and Vibration* 543 (2023) 117355. <http://dx.doi.org/10.1016/j.jsv.2022.117355>.
- G.D. Töpfer: Die Theorie und Praxis des Orgelbaus (The theory and practice of organ building). Bernhard Friedrich Voigt, Weimar, 1888. In German.
- F. Ingerslev, W. Frobenius: Some measurements of the end-corrections and acoustic spectra of cylindrical open flue organ pipes. *Transactions of the Danish Academy of Technical Sciences* 1, 3 (1947) 1–42.
- N.H. Fletcher: Sound production by organ flue pipes. *Journal of the Acoustical Society of America* 60 (1976) 1119–1132. <http://dx.doi.org/10.1121/1.381174>.
- M.E. McIntyre, R.T. Schumacher, J. Woodhouse: On the oscillations of musical instruments. *Journal of the Acoustical Society of America* 74, 5 (1983) 1325–1345. <http://dx.doi.org/10.1121/1.390157>.
- M.P. Verge, B. Fabre, W.E.A. Mahu, A. Hirschberg, R.R. van Hassel, A.P.J. Wijnands, J.J. de Vries, C.J. Hogendoorn: Jet formation and jet velocity fluctuations in a flue organ pipe. *Journal of the Acoustical Society of America* 95, 2 (1994) 1119–1132. <http://dx.doi.org/10.1121/1.408460>.
- B. Fabre, J. Gilbert, A. Hirschberg, X. Pelorson: Aeroacoustics of musical instruments. *Annual Review of Fluid Mechanics* 44, 1 (2012) 1–25. <http://dx.doi.org/10.1146/annurev-fluid-120710-101031>.
- P.T. Nagy, P. Rucz, A. Szabó: Examination of jet growth and jet-drive in the recorder by means of linearized numerical and lumped models. *Journal of Sound and Vibration* 527 (2022) 116857. <http://dx.doi.org/10.1016/j.jsv.2022.116857>.
- S. Dequand, J.F.H. Willems, M. Leroux, R. Vullings, M. van Weert, C. Thielout, A. Hirschberg: Simplified models of flue instruments: influence of mouth geometry on the sound source. *Journal of the Acoustical Society of America* 113, 3 (2003) 1724–1735. <http://dx.doi.org/10.1121/1.1543929>.
- J. Angster, G. Paál, W. Garen, A. Miklós: Effect of voicing steps on the stationary spectrum and attack transient of a flue organ pipe, in: *Proceedings of the International Symposium on Musical Acoustics*. Institute of Acoustics, Edinburgh, Vol. 19, Part 5, Book 2, 1997, pp. 285–294.
- R. Janke: The secret of scaling. *ISO Journal* 49 (2015) 50–64. <https://www.orgel-info.de/Mensuren.pdf>.
- INNOSOUND – Innovative methods and tools for the sound design of organ pipes. Research project in the 7th Framework Program of the European Union; Research for SME (FP7-SME-2007-1), 2008–2010. Contract no: INNOSOUND-222104.
- P. Rucz, E. Esteve Fontestad, J. Angster, A. Miklós: An improved scaling method for wooden flue organ pipes, in: A. Astolfi, F. Asdrudali, L. Shtrepi (Eds) *Forum Acusticum 2023: Proceedings of the 10th Convention of the European Acoustics Association*, 2023, pp. 4447–4454. <http://dx.doi.org/10.61782/fa.2023.0917>.
- S. Tateishi, S. Iwagami, G. Tsutsumi, T. Kobayashi, T. Takami, K. Takahashi: Role of the foot chamber in the sounding mechanism of a flue organ pipe. *Acoustical Science and Technology* 40, 1 (2019) 29–39. <http://dx.doi.org/10.1250/ast.40.29>.
- S. Ikoga, T. Onomata, R. Tabata, S. Iwagami, T. Kobayashi, K. Takahashi: Numerical study on a three-dimensional model of a flue organ pipe: relative phase between pipe and foot, and stability, in: A. Astolfi, F. Asdrudali, L. Shtrepi (Eds.) *Forum Acusticum 2023: Proceedings of the 10th Convention of the European Acoustics Association*, 2023, pp. 4439–4442. <http://dx.doi.org/10.61782/fa.2023.0425>.
- R. Caussé, J. Kergomard, X. Lurton, Input impedance of brass instruments – Comparison between experiment and numerical models. *Journal of the Acoustical Society of America* 75, 1 (1984) 241–254. <http://dx.doi.org/10.1121/1.390402>.
- A.H. Benade: On the propagation of sound waves in a cylindrical conduit. *Journal of the Acoustical Society of America* 44, 2 (1968) 616–623. <http://dx.doi.org/10.1121/1.1911130>.

25. M. Berggren, A. Bernland, D. Noreland, Acoustic boundary layers as boundary conditions. *Journal of Computational Physics* 371 (2018) 633–650. <http://dx.doi.org/10.1016/j.jcp.2018.06.005>.
26. Mathworks Inc.: Documentation of `lsqnonlin`: solve nonlinear least-squares (nonlinear data-fitting) problems. Last accessed: 19 February, 2024. <https://de.mathworks.com/help/optim/ug/lsqnonlin.html>.
27. I. Harari: Dispersion, pollution, and resolution, in: S. Marburg, B. Nolte (Eds.) *Computational Acoustics of Noise Propagation in Fluids – Finite and Boundary Element Methods*. Springer, Berlin, Chapter 1, 2008, 37–56.
28. Openwind: Python library assisting instrument makers. Last accessed: 23 September, 2024. <https://openwind.inria.fr/>.
29. C. Geuzaine, J.-F. Remacle: Gmsh: a three-dimensional finite element mesh generator with built-in pre- and post-processing facilities. *International Journal for Numerical Methods in Engineering* 79, 11 (2009) 1309–1331. <http://dx.doi.org/10.1002/nme.2579>.
30. R.J. Astley, G.J. Macaulay, J.-P. Coyette, L. Cremers: Three-dimensional wave-envelope elements of variable order for acoustic radiation and scattering: Part I. Formulation in the frequency domain. *Journal of the Acoustical Society of America* 103 (1998) 49–63. <http://dx.doi.org/10.1121/1.421106>.
31. J. Angster, P. Rucz, A. Miklós: Acoustics of organ pipes and future trends in the research. *Acoustics Today* 13, 1 (2017) 12–20.
32. S. Adachi: A simple model of cross-fingering explaining both pitch flattening and sharpening. *Journal of the Acoustical Society of America* 140, 4 (2016) 3426–3427. <http://dx.doi.org/10.1121/1.4971029>.
33. S. Adachi: Resonance modes of a flute with one open tone hole. *Acoustical Science and Technology* 38, 1 (2017) 14–22.
34. H. Außerlechner, T. Trommer, J. Angster, A. Miklós: Experimental jet velocity and edge tone investigations on a foot model of an organ pipe. *Journal of the Acoustical Society of America* 126, 2 (2009) 878–886. <http://dx.doi.org/10.1121/1.3158935>.
35. G. Paál, I. Vaik: Unsteady phenomena in the edge tone. *International Journal of Heat and Fluid Flow* 28 (2007) 575–586. <http://dx.doi.org/10.1016/j.ijheatfluidflow.2007.04.011>.

Cite this article as: Rucz P. Esteve Fontestad E. Angster J. & Miklós A. 2025. Wall losses in straight ducts with non-circular cross sections: a scaling rule of identical losses for wooden flue organ pipes. *Acta Acustica*, 9, 10. <https://doi.org/10.1051/aacus/2024084>.